APPLICATION OF 2D ACOUSTIC FULL WAVEFORM INVERSION TO OBC-DATA

M. Kunert, A. Kurzmann, and T. Bohlen

email: *markus.kunert@student.kit.edu, kurzmann@kit.edu*
keywords: *acoustic full waveform inversion, time-domain, marine field data*

ABSTRACT

In exploration geophysics it is important to characterise the subsurface – in particular oil and gas deposits – as good as possible. Full waveform inversion (FWI) exploits the full content of seismic data in order to reconstruct parameter models at sub-wavelength scales. It helps to improve the seismic and petrophysical interpretation by assigning physical parameters to structural images obtained by classical methods. In this work we applied 2D acoustic FWI in the time domain to a marine seismic data set acquired in a river delta area using ocean bottom cables. Based on particular circumstances, such as the occurrence of guided waves in shallow water and a simple starting model for the P-wave velocity, we developed a comprehensive inversion strategy involving data windowing (with focus on refracted waves), data filtering and an alternating inversion for model parameter and source signature. This complex FWI workflow has been successfully applied to the field data set, resulting in the reconstruction of a velocity model showing small-scale structures. In particular, we identified low-velocity areas as potential fault zones or gas "pockets". The comparison of the FWI model with the result of a standard reflection seismic imaging method shows a high similarity. On the one hand, this can be considered as a validation of the FWI strategy. On the other hand, the availability of structural information and physical parameters improves petrophysical characterisation of the subsurface.

INTRODUCTION

The full waveform inversion (FWI) is an efficient method to resolve complex subsurface structures. In contrast to conventional ray tracing methods, used in marine seismics, FWI is able to use the full content of the observed seismic data, i. e., amplitudes and phases. Hence, FWI has the potential to focus on structures at or below the wavelength. First, the large-scale structures need to be estimated by conventional methods, such as the traveltime tomography. FWI efforts a huge ammount of computer resources which is part of the reason why it is not a common practice yet.

In this work, we apply the 2D acoustic FWI in the time domain to marine seismic data. We intend to resolve small-scale gas accumulations which may occur in the investigated area and cause difficulties for standard seismic imaging methods. Similar gas accumulations are already resolved by application of viscoacoustic waveform inversion by Hicks and Pratt (2001). One of the first application to marine seismic data was presented by Crase et al. (1990). In case of marine seismic data the acoustic approximation seems to be sufficient and saves computational resources. Due to the potential existence of gas accumulations and weakly consolidated rocks, we apply FWI in the acoustic approximation with consideration of attenuation as a modelling parameter.

FULL WAVEFORM INVERSION

The theory of acoustic FWI summarized in Kurzmann (2012) was presented in the previous annual WIT reports. The works of Köhn et al. in 2008 and 2009 as well as Kurzmann et al. (e. g., in 2008 and 2011) explain the theoretical backround. The first application to real data is given by Przebindowska et al. (e. g., in 2010 and 2011).

The inversion algorithm is mainly based on the theory of Tarantola (1984) and Mora (1987). The full waveform inversion aims to estimate a subsurface model, which is able to explain the seismic recordings by iterative minimization of the residuals between the observed and modelled data. Full waveform inversion consists of two main tasks. First, the forward modelling problem needs to be solved with a current model. A set of physical parameters, such as seismic velocity, density or attenuation, is chosen to represent the characteristics of a subsurface. The viscoacoustic wave equation is solved using time-domain finite-difference method. The second task is an inverse problem of finding model parameters from the observed data. The difference between the observed and forward modelled data is minimized. This is done by an iterative adjoint gradient method. The final subsurface model which explains the observed data is assumed to be similar to the true subsurface.

ACQUISITION GEOMETRY AND FIELD DATA

Acquisition geometry

The field data was acquired in a river delta in order to characterise an oil and gas deposit. However, object of this work is the near surface region, where rising gases may strike to impenetrable sediments, such as layers of clay. The gases accumulate and reduce the seismic velocities, which may be detected by FWI. The data set was acquired in an OBC-geometry (Ocean Bottom Cable) shown in figure 1. The receivers were placed at the sea floor whereas the source array was dragged by a ship and triggered near the surface in 6 m depth. The main acquisition parameters are listed in table 1.

Field data example

The hydrophones recorded the time derivation of the pressure sampled with 500 Hz. An exemplary seismogram is shown in figure 2(a). It contains frequencies up to 230 Hz demonstrated by the mean amplitude spectrum in figure 2. However, in application of FWI especially the low frequencies and a sequential increase of frequency content are important (Bunks et al., 1995). Suitable frequencies start at 3 Hz. Because of noise signals around 0.5 Hz a bandpass filter is required. An exemplary band pass filtered seismogram is shown in figure 3(b) and exposes a specific feature of seismic measurements in shallow water. Due to a relatively thin water layer and a strong seismic contrast at the sea floor, a significant amount of seismic energy may be trapped inside the water column, resulting in strong "guided waves" (e. g., Klein et al., 2005). The required conditions to simulate these guided waves were not fulfilled by the forward solver. Consequently, we decided to apply a particular FWI workflow described in section "WORKFLOW".

Table 1: Acquisition parameters used in field-data measurement

Number of shots	61
Shot depth	6 m
Shot point interval	200 m
Number of hydrophones	240
Hydrophone depth	122 m - 146 m
Hydrophone interval	25 m
Profile length	12 km
Offsets	118 m - 8993 m
Record length	6 s
Sample interval	2 ms
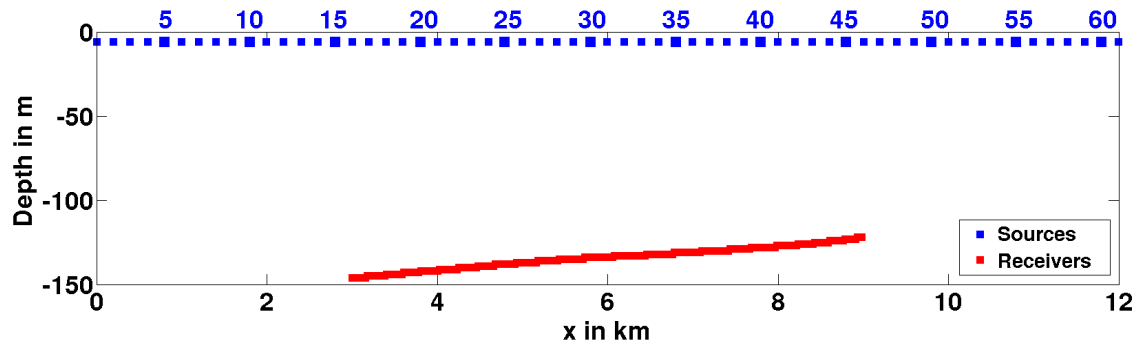
Figure 1: The 2D approximated OBC acquisition geometry. The sources (blue) were triggered near the surface in 6 m depth. The hydrophones (red) were located at the sea floor.

(a)
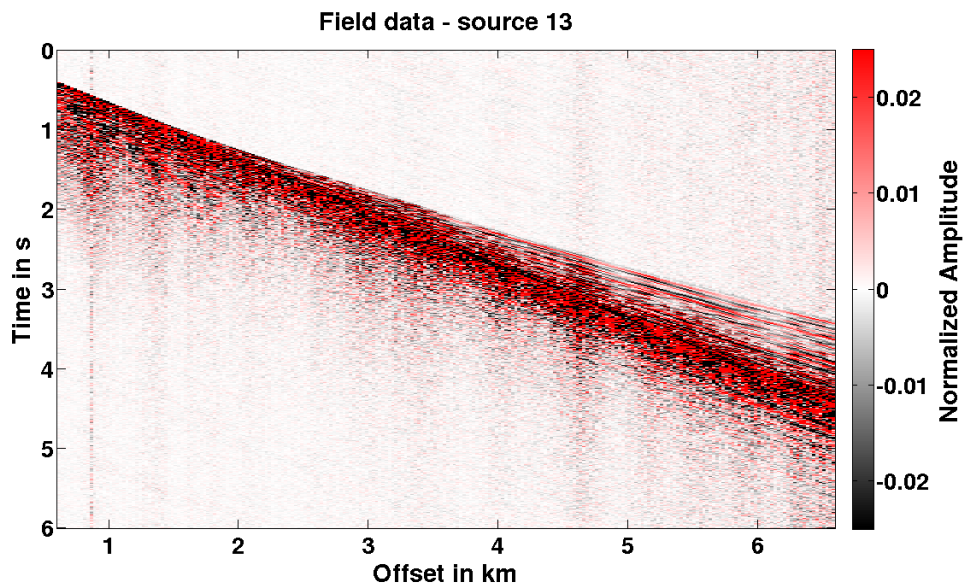
(b)
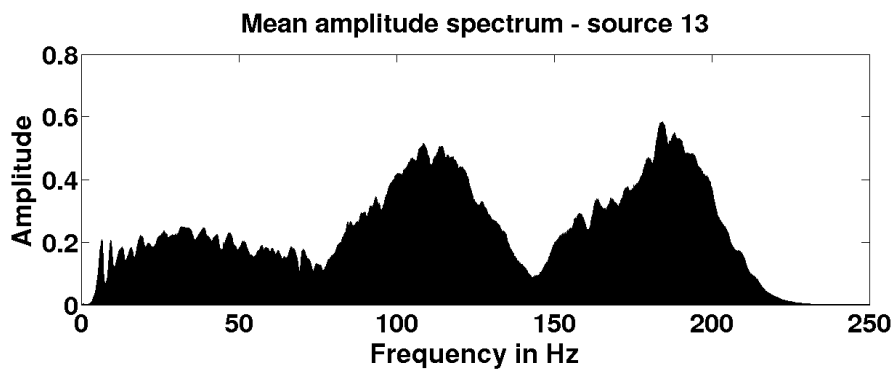
Figure 2: (a) Exemplary field data normalized to the particular trace maximum. (b) Mean amplitude spectrum of the raw field data. The 240 traces were normalized to the particular maximum and averaged to the displayed mean spectrum.

(a)

(b)

(c)
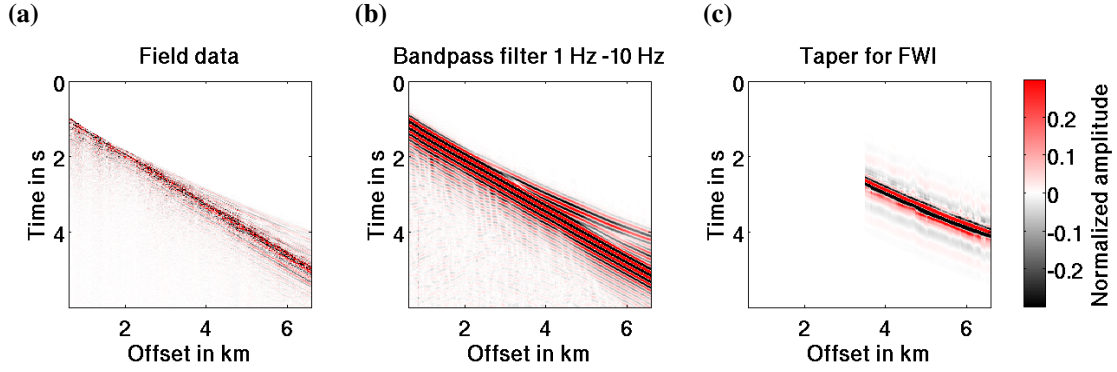
Figure 3: (a) Exemplary field data seismogram. (b) Filtered field data seismogram. (c) Tapered and filtered field data seismogram (used in full waveform inversion). The seismograms belong to the source position 13 and were normalized to the respective trace maxima.

PREREQUISITES FOR FWI

Starting model

In this work, we used the result of a traveltime tomography as a v_p starting model (see figure 4). It contains only large-scale structures representing very low frequencies which are not available in the seismic data. An estimation of a density model based on the velocity model results from Gardner et al. (1974),

$$\rho \,(\text{in kg/m}^3) \approx 310 \cdot v_p^{0.25}, \tag{1}$$

and is shown in figure 4. The density is not subject to the inversion, but will be updated in each iteration to the particular v_p model using the equation 1.

The acquisition took place in a river delta. Thus, we assume significant attenuation caused by unconsolidated sediments. In order to take these attenuation effects better into account, we generated an attenuation model to be used in the forward modelling. We estimated a homogeneous quality factor model with $Q_p = 50$ for the sediments and acoustic conditions in the water layer.

Although we are interested in the shallow areas, a model depth of 2200 m is necessary to provide the simulation of refracted waves from greater depths.

Modelling parameters

The spatial grid point distance Δh needs to fulfil the requirements of the used finite difference method. To reduce grid dispersion Köhn (2011) recommends $m = 12$ grid points per wavelength in case of the second order finite difference operator used in this work. We evaluate frequencies up to 30 Hz and exclude velocites below $1000\,\frac{\text{m}}{\text{s}}$. According to Köhn (2011) a spatial grid point distance of

$$\Delta h \leq \frac{v_{p,min}}{m\,f_{max}} = \frac{1000\,\frac{\text{m}}{\text{s}}}{12 \cdot 30\,\text{Hz}} \approx 2.78\,\text{m} \tag{2}$$

is required which is why we chose a grid point distance of $\Delta h = 2.5\,\text{m}$. Hence, according to the Courant condition (Courant et al., 1928) the time sampling Δt should not exceed

$$\Delta t \leq \frac{\Delta h}{\sqrt{2}\,v_{p,max}} = \frac{2,5\,\text{m}}{\sqrt{2} \cdot 3500\,\frac{\text{m}}{\text{s}}} \approx 5 \cdot 10^{-4}\,\text{s}. \tag{3}$$

Therefore we specified a time sampling of $\Delta t = 4.5 \cdot 10^{-4}\,\text{s}$. The resulting finite-difference scheme comprises 13333 time steps (to consider the full record length) and physical models with a size of 4864×880 grid points.
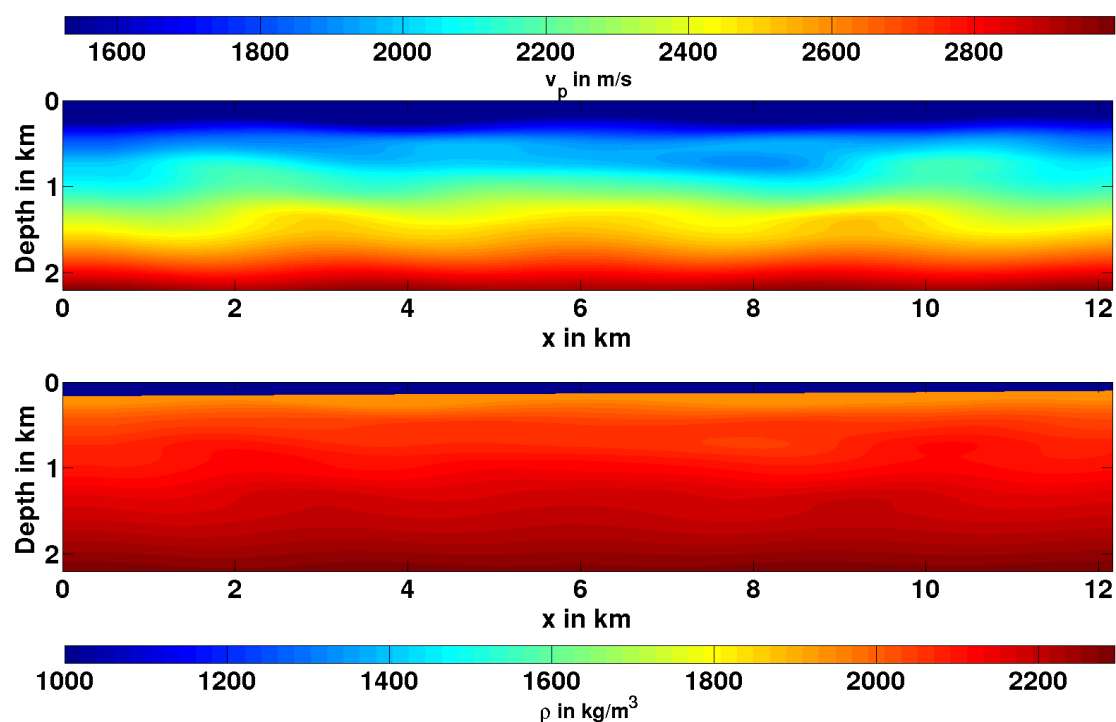
Figure 4: Starting model for P-wave velocity v_p (top) and density (bottom). Models are based on a provided traveltime tomography.

Source wavelet

An accurate estimation of the source wavelet is an cruical issue to be able to explain the recorded field data by the forward modelled synthetic data. In our implementation, we apply a source-wavelet inversion based on the least-squares method by Pratt (1999).

WORKFLOW – INVERSION STRATEGY

An accurate inversion strategy is essential for the success of FWI. It is represented by complex inversion workflow consisting of several stages with particular instructions, such as:

- **Number of iterations:** Determines the minimum number of iterations to perform for this current workflow stage.

- **Stop criterion:** Specifies the progress after reaching the minimum number of requested iterations. It is possible to continue with the current workflow stage until the model updates stop improving the misfit. A minimum requested misfit improvement may be defined by this instruction. Additionally, it is possible to immediately start with the next workflow stage.

- **Subject of the inversion:** It is possible to choose between an inversion of the model parameter and the source wavelet.

- **Taper:** Specifies the instructions for application of time and offset windows.

- **Frequency filter:** Define the frequency content to be considered.

The general inversion scheme is illustrated in figure 5. In everey iteration step the specified workflow instructions are applied to each source. The forward modelling is followed by the time and offset tapering. Afterwards, a band-pass filter is applied in order to obtain the desired frequency content. Depending on the inversion subject, the misfit should be reduced by updates of the source wavelet or the subsurface model.

Input:
- observed data
- initial parameter model
- initial source wavelet

At iteration k
Read current work instuctions from workflow file:
- stop criterion
- subject of inversion (source wavelet or model parameter)
- parameters of time and offset taper

For each source

Forward modelling: solve wave equation and calculate modelled data

Apply time and offset taper to observed and modelled data

Apply frequency filter to observed and modelled data

Inversion for model parameter

Inversion for source wavelet

- calculation of residuals and misfit
- back propagation and calculation of gradients
- preconditioning of gradients

- Calculation of the source wavelet is based on the least squares method.

next iteration $k + 1$

No   Misfit minimized?   Yes

Stop:
best-fit model
has been found

No   Is workflow finished?   Yes: next workflow step

Summation of gradients

Preconditioning und calculation of step length

Update model parameter

Figure 5: Adaption of the full waveform inversion scheme shown in Kurzmann (2012).

As the misfit function of the full waveform inversion problem gets more complex with increasing frequencies it is common procedure to start with low frequencies. Higher frequencies are added after several iterations to increase the regarded informational content and gain detailed informations about the subsurface. However, the guided water waves could not be modelled correctly. Thus, a time taper is required. Only the first cycles after the first arrivals are taken into account. The length of the specified time window needs to match to the observed frequency content. Hence, the window length will be shortened with increasing frequencies. As the first arrivals of the direct water wave do not carry informations about the subsurface, we focus on the far offsets. As a consequence, we ignored central sources (source numbers 26 to 36). Furthermore, we observed difficulties at near offsets due to inevitable interference of the direct wave with the guided water wave within the defined time window. The application of an offset taper allows the focus on offsets larger than 3500 m as shown in figure 3(c). Finally, the data reduction to refracted waves in a subset of workflow stages helpes to stabilize FWI and to improve the resulting parameter model. The detailed workflow is listed in the table 2.

INVERSION RESULTS

Exemplary seismograms in figure 6 show, that FWI was able to find a subsurface model explaining observed data. The refracted waves of both observed data and final synthetic data match quite well. The FWI progress is characterized by a continuously reduced data misfit (figure 7) within each frequency range. Source-wavelet inversions are performed at the beginning of every frequency range. Additionally, the source signal is updated two more times within each frequency range. Due to the usage of the initial source signal, we observe significant misfit peaks (red dots in figure 7). The source wavelets of all sources obtained at the end of the FWI application are shown in figure 8. They show a comparable waveform and, thus, satisfactorily represent the robustness of the inversion strategy – assuming consistency of the source array in generating similar signatures. However, some source signals show stronger differences in amplitude and phase (comparing sources in the center of the model and sources at the ends of the model). Possible reasons might be an insufficient illumination of some model areas, a simple assumption of the quality factor of the viscoacoustic medium and neglecting more complex effects of wave propagation.

The final v_p model is shown in figure 9(a). Most of the recovered geological structures are located within the dashed rectangle. The side areas of the model as well as greater depths of the model are poorly illuminated. However, we achieved a satisfactory resolution in the centre of the model (relates to $3\,\text{km} \leq x \leq 9\,\text{km}$), i. e., FWI reconstructed structures at (sub-)wavelength scale (using dominant frequency of approximately 15 Hz) in the area beneath the receiver array. Layered structures could be identified in shallow parts. As mentioned previously, rising gases in that area may form accumulations and reduce the seismic velocities. Therefore, the low-velocity zones are of particular interest. Some of the dipping low-velocity structures may refer to fault zones which enable gases to rise up. Along the fault zones some rock structures may allow the accumulation of gases – forming low-velocity "pockets", particularly at shallow areas close to the sea floor.

We validated the quality of the velocity model by comparison with the result of a conventional reflection seismic imaging method shown in figure 9(b). Disregarding a different content of wavelengths or frequencies, respectively, they show a very good match, in particular fault zones and areas of strong seismic contrasts, such as gas accumulations.

CONCLUSION

In this work, we presented a complex strategy to allow a successful application of the acoustic full waveform inversion in the time domain to marine seismic field data. Based on a simple starting model, small-scale structures, such as fault zones or other low-velocity areas with gas accumulations, could be recovered. Due to the occurrence of strong guided waves in the shallow water, which could not be explained sufficiently by seismic modelling, we focused on refracted waves. Consequently, we implemented and applied a nested workflow involving time windowing, offset windowing and frequency filtering. Although we only considered a fraction of the data, full waveform inversion was able to obtain a velocity model which shows a high similarity to the result of a conventional reflection seismic imaging method. Both methods combine

Table 2: FWI workflow consisting of several stages (lines) and according instructions (rows).

Iteration		Frequency	Length of time window	Offsets
1	source inversion	1 - 4 Hz	6 s	0 - 9000 m
2 - 12	v_p-inversion		0,4 s	0 - 9000 m
13	source inversion		6 s	0 - 9000 m
14 - 24	v_p-inversion		0,4 s	3500 - 9000 m
25	source inversion		6 s	0 - 9000 m
26 - 46	v_p-inversion		0,4 s	3500 - 9000 m
47	source inversion	1 - 7 Hz	6 s	0 - 9000 m
48 - 58	v_p-inversion		0,25 s	0 - 9000 m
59	source inversion		6 s	0 - 9000 m
60 - 70	v_p-inversion		0,25 s	3500 - 9000 m
71	source inversion		6 s	0 - 9000 m
72 - 92	v_p-inversion		0,25 s	3500 - 9000 m
93	source inversion	1 - 10 Hz	6 s	0 - 9000 m
94 - 104	v_p-inversion		0,2 s	0 - 9000 m
105	source inversion		6 s	0 - 9000 m
106 - 116	v_p-inversion		0,2 s	3500 - 9000 m
117	source inversion		6 s	0 - 9000 m
118 - 138	v_p-inversion		0,2 s	3500 - 9000 m
139	source inversion	1 - 15 Hz	6 s	0 - 9000 m
140 - 150	v_p-inversion		0.15 s	0 - 9000 m
151	source inversion		6 s	0 - 9000 m
152 - 164	v_p-inversion		0.15 s	3500 - 9000 m
165	source inversion		6 s	0 - 9000 m
166 - 186	v_p-inversion		0.15 s	3500 - 9000 m
187	source inversion	1 - 19 Hz	6 s	0 - 9000 m
188 - 198	v_p-inversion		0.15 s	0 - 9000 m
199	source inversion		6 s	0 - 9000 m
200 - 210	v_p-inversion		0.15 s	3500 - 9000 m
211	source inversion		6 s	0 - 9000 m
212 - 232	v_p-inversion		0.15 s	3500 - 9000 m
233	source inversion	1 - 25 Hz	6 s	0 - 9000 m
234 - 244	v_p-inversion		0,15 s	0 - 9000 m
245	source inversion		6 s	0 - 9000 m
246 - 266	v_p-inversion		0,15 s	3500 - 9000 m
267	Quellinversion		6 s	0 - 9000 m
268 - 288	v_p-inversion		0,15 s	3500 - 9000 m
289	source inversion	1 - 30 Hz	6 s	0 - 9000 m
290 - 300	v_p-Inversion		0,13 s	0 - 9000 m
301	Quellinversion		6 s	0 - 9000 m
302 - 312	v_p-Inversion		0,13 s	3500 - 9000 m
313	Quellinversion		6 s	0 - 9000 m
314 - 324	v_p-Inversion		0,13 s	3500 - 9000 m
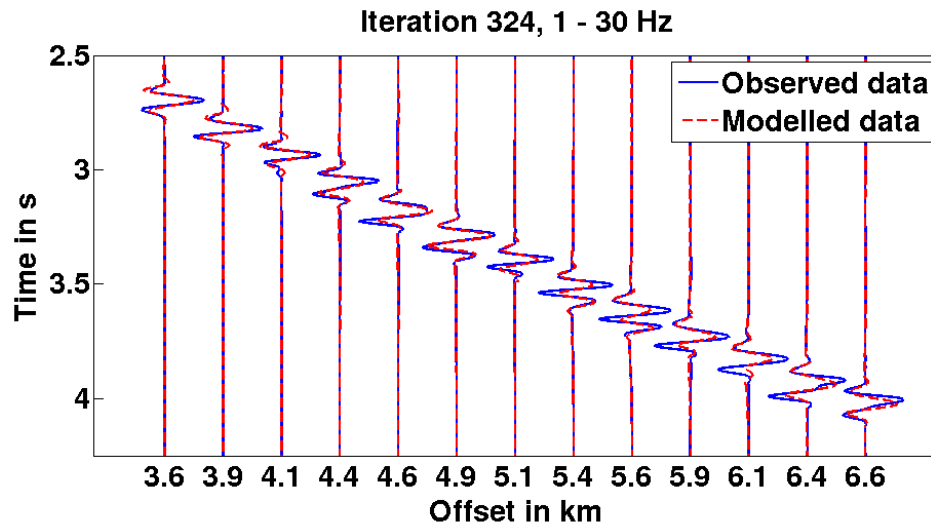
Figure 6: Exemplary seismic traces display the final fit between observed and modelled data. The traces were normalized to the particular maximum of the observed data and originate from source 13.
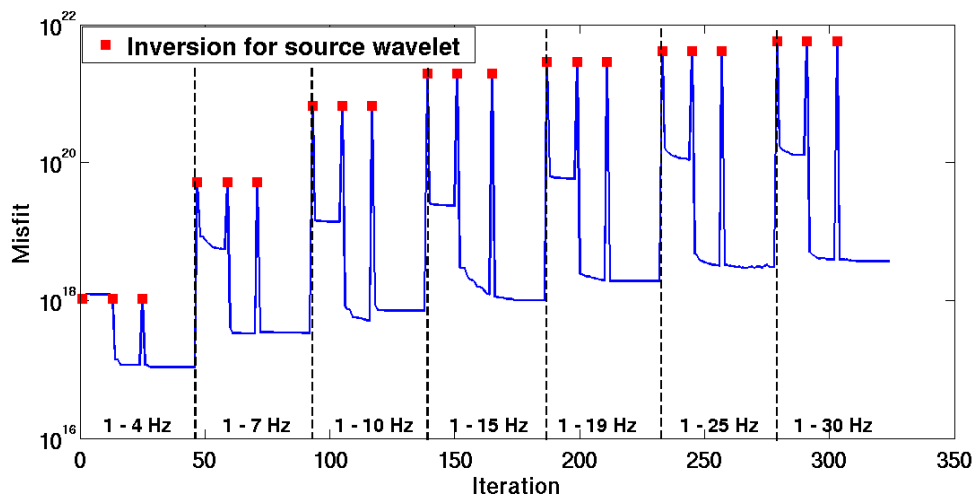
Figure 7: Progress of the misfit value for the applied full waveform inversion. The red marks indicate the iteration with a source wavelet inversion.

structural information of the subsurface and physical parameters, such as the velocity of the compressional wave, which is an important step for further petrophysical characterisation.

REFERENCES

Bunks, C., Saleck, F. M., Zaleski, S., and Chavent, G. (1995). Multiscale seismic waveform inversion. *Geophysics*, 60(5):1457–1473.

Courant, R., Friedrichs, K., and Lewy, H. (1928). Über die partiellen differenzengleichungen der mathematischen physik. *Mathematische Annalen*, 100(1):32–74.

Crase, E., Pica, A., Noble, M., McDonald, J., and Tarantola, A. (1990). Robust elastic nonlinear waveform inversion: Application to real data. *Geophysics*, 55(5):527–538.

Gardner, G., Gardner, L., and Gregory, A. (1974). Formation velocity and density-the diagnostic basics for stratigraphic traps. *Geophysics*, 39(6):770–780.

Hicks, G. J. and Pratt, R. G. (2001). Reflection waveform inversion using local descent methods: Estimating attenuation and velocity over a gas-sand deposit. *Geophysics*, 66(2):598–612.

Klein, G., Bohlen, T., Theilen, F., Kugler, S., and Forbriger, T. (2005). Acquisition and inversion of dispersive seismic waves in shallow marine environments. *Marine Geophysical Researches*, 26(2-4):287–315.

Köhn, D. (2011). Time domain 2D elastic full waveform tomography. *Ph. D. dissertation*.
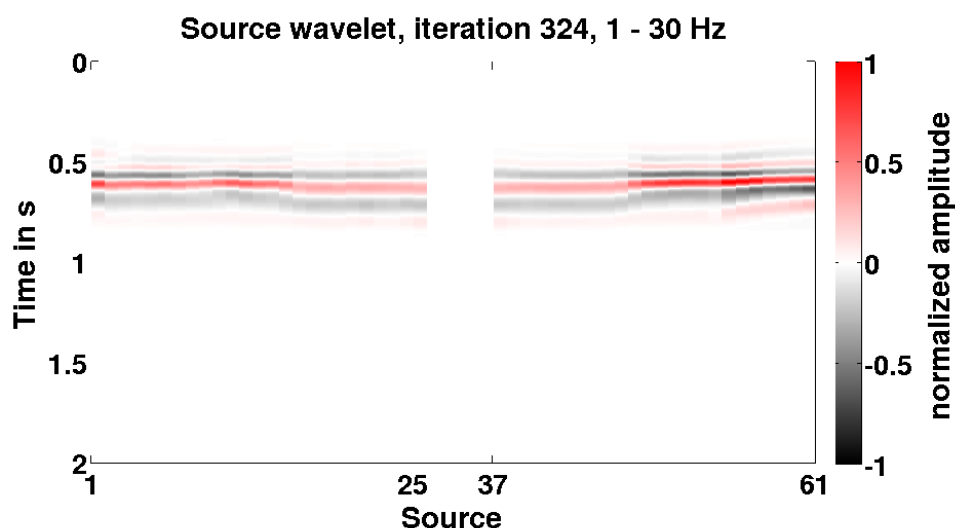
Figure 8: Source wavelets used in the forward modelling of the final iteration step. The amplitudes are normalized to the overall maximum.

(a)

(b)
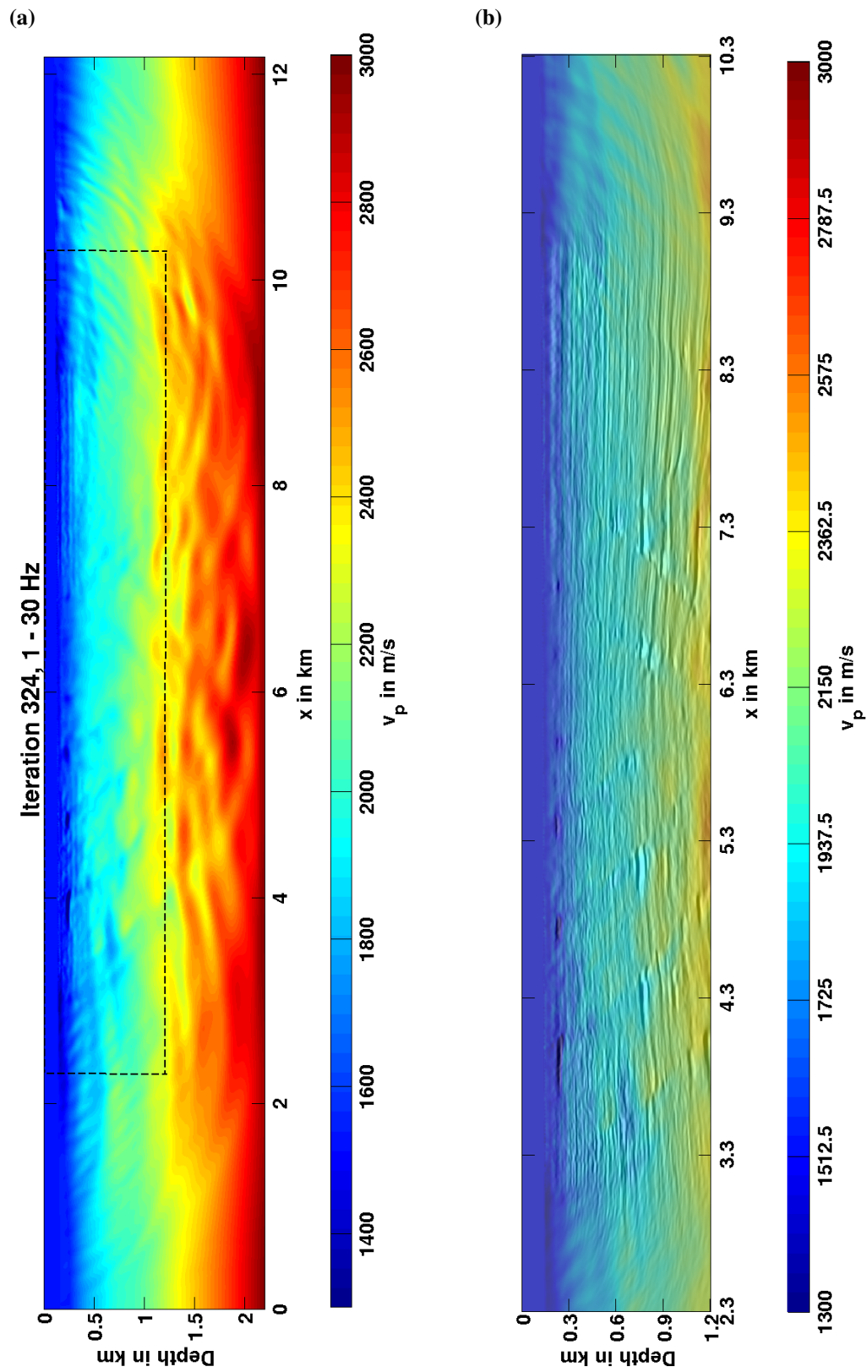
Figure 9: (a) Final v_p model obtained from FWI. The dashed rectangle marks the section shown below. (b) Overlapping of the final v_p model with the provided result of a reflection seismic imaging method.

Kurzmann, A. (2012). *Applications of 2D and 3D full waveform tomography in acoustic and viscoacoustic complex media*. PhD thesis, Karlsruher Institut für Technologie.

Mora, P. (1987). Nonlinear two-dimensional elastic inversion of multioffset data. *Geophysics*, 52(9):1211–1228.

Pratt, R. (1999). Seismic waveform inversion in the frequency domain, part 1: Theory and verification in a physical scale model. *Geophysics*, 64:888–901.

Tarantola, A. (1984). Inversion of seismic reflection data in the acoustic approximation. *Geophysics*, 49:1259–1266.